

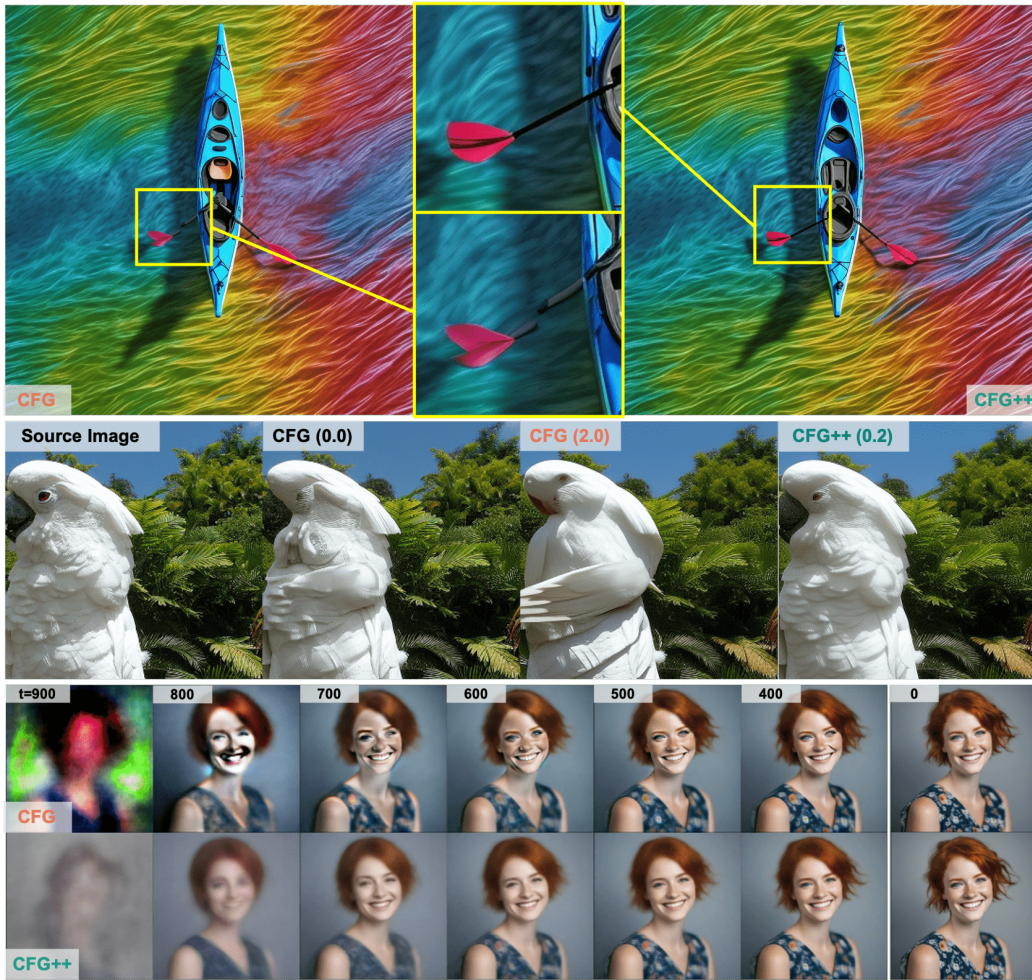
CFG++: MANIFOLD-CONSTRAINED CLASSIFIER FREE GUIDANCE FOR DIFFUSION MODELS

Hyungjin Chung*, Jeongsol Kim*, Geon Yeong Park*, Hyelin Nam*, Jong Chul Ye

KAIST

*: Equal Contribution

{hj.chung, jeongsol, pky3436, hyelin.nam, jong.ye}@kaist.ac.kr



"beautiful lady, freckles, big smile, blue eyes, short ginger hair, wearing a floral blue vest top, soft light, dark gray background"

Figure 1: **(Top)** Comparison of T2I results by SDXL for the prompt "kayak in the water, optical color, aerial view, rainbow". The CFG-guided image has a broken oar, an artifact significantly reduced in the CFG++ version. **(Middle)** DDIM Inversion results show noticeable artifacts at various CFG scales, which are significantly reduced by CFG++. **(Bottom)** The evolution of denoised estimates differs between CFG and CFG++. CFG exhibits sudden shifts and intense color saturation early in reverse sampling, while CFG++ transitions smoothly from low to high-resolution details.

ABSTRACT

Classifier-free guidance (CFG) is a fundamental tool in modern diffusion models for text-guided generation. Although effective, CFG has notable drawbacks. For instance, DDIM with CFG lacks invertibility, complicating image editing;

furthermore, high guidance scales, essential for high-quality outputs, frequently result in issues like mode collapse. Contrary to the widespread belief that these are inherent limitations of diffusion models, this paper reveals that the problems actually stem from the off-manifold phenomenon associated with CFG, rather than the diffusion models themselves. More specifically, inspired by the recent advancements of diffusion model-based inverse problem solvers (DIS), we reformulate text-guidance as an inverse problem with a text-conditioned score matching loss, and develop CFG++, a novel approach that tackles the off-manifold challenges inherent in traditional CFG. CFG++ features a surprisingly simple fix to CFG, yet it offers significant improvements, including better sample quality for text-to-image generation, invertibility, smaller guidance scales, reduced mode collapse, etc. Furthermore, CFG++ enables seamless interpolation between unconditional and conditional sampling at lower guidance scales, consistently outperforming traditional CFG at all scales. Experimental results confirm that our method significantly enhances performance in text-to-image generation, DDIM inversion, editing, and solving inverse problems, suggesting a wide-ranging impact and potential applications in various fields that utilize text guidance. Project Page: <https://cfgpp-diffusion.github.io/>.

1 INTRODUCTION

Classifier-free guidance (CFG) (Ho & Salimans, 2021) forms the key basis of modern text-guided generation with diffusion models (Dhariwal & Nichol, 2021; Rombach et al., 2022). Nowadays, it is common practice to train a diffusion model with large-scale paired text-image data (Schuhmann et al., 2022), so that sampling (i.e. generating) a signal (e.g. image, video) from a diffusion model can either be done unconditionally from $p_\theta(\mathbf{x}|\emptyset) \equiv p_\theta(\mathbf{x})$, or conditionally from $p_\theta(\mathbf{x}|c)$, where c is the text conditioning. Once trained, it seems natural that one would acquire samples from the conditional distribution by simply solving the probability-flow ODE or SDE sampling (Song et al., 2021b;a; Karras et al., 2022) with the conditional score function. In practice, however, it is observed that the conditioning signal is insufficient when used naively. To emphasize the guidance, one uses the guidance scale $\omega > 1$, where the direction can be defined by the direction from the unconditional score to the conditional score (Ho & Salimans, 2021).

In modern text-to-image (T2I) diffusion models, the guidance scale ω is typically set within the range of [5.0, 30], referred to as the *moderately* high range of CFG guidance (Chen et al., 2024b; Podell et al., 2023). The insufficiency in guidance also holds for classifier guidance (Dhariwal & Nichol, 2021; Song et al., 2021b) so that a scale of 10 was used. While using a high guidance scale yields higher-quality images with better alignment to the condition, it is also prone to mode collapse, reduces sample diversity, and yields an inevitable accumulation of errors during the sampling process. One example is DDIM inversion (Dhariwal & Nichol, 2021), a pivotal technique for controllable synthesis and editing (Mokady et al., 2023), where running the inversion process with $\omega > 1.0$ leads to significant compromise in the reconstruction performance (Mokady et al., 2023; Wallace et al., 2023). Another extreme example would be score distillation sampling (SDS) (Poole et al., 2022), where the guidance scale in the order of a few hundred is chosen. Using such a high guidance scale leads to better asset quality to some extent, but induces blurry and saturated results. Several research efforts have been made to mitigate this downside by exploring methods where using a smaller guidance scale suffices (Wang et al., 2024; Liang et al., 2023). Although recent progress in SDS-type methods has reduced the necessary guidance scale to a range that is similar to those of ancestral samplers, using a moderately large ω is considered an inevitable choice.

In this work, we aim to give an answer to this conundrum by revisiting the geometric view of diffusion models. In particular, inspired by the recent advances in diffusion-based inverse problem solvers (DIS) (Kadkhodaie & Simoncelli, 2021; Chung et al., 2023a; Song et al., 2023a; Kim et al., 2024; Chung et al., 2024), we reformulate the text-guidance as an inverse problem with a text-conditioned score matching loss and derive reverse diffusion sampling strategy by utilizing the decomposed diffusion sampling (DDS) (Chung et al., 2024). This results in a surprisingly simple fix of CFG to the sampling process without any computational overhead. The resulting process, which we call CFG++, works with a small guidance scale, typically $\lambda \in [0.0, 1.0]$, that smoothly *interpolates* between unconditional and conditional sampling, with $\lambda = 1.0$ having a similar effect as using CFG sampling with $\omega \sim 12.5$ at 50 neural function evaluation (NFE). Furthermore, DDIM inversion with CFG++

Algorithm 1 Reverse Diffusion with CFG	Algorithm 2 Reverse Diffusion with CFG++
Require: $\mathbf{x}_T \sim \mathcal{N}(0, \mathbf{I}_d)$, $0 \leq \omega \in \mathbb{R}$ 1: for $i = T$ to 1 do 2: $\hat{\epsilon}_c^\omega(\mathbf{x}_t) = \hat{\epsilon}_\emptyset(\mathbf{x}_t) + \omega[\epsilon_c(\mathbf{x}_t) - \hat{\epsilon}_\emptyset(\mathbf{x}_t)]$ 3: $\hat{\mathbf{x}}_c^\omega(\mathbf{x}_t) \leftarrow (\mathbf{x}_t - \sqrt{1 - \bar{\alpha}_t} \hat{\epsilon}_c^\omega(\mathbf{x}_t)) / \sqrt{\bar{\alpha}_t}$ 4: $\mathbf{x}_{t-1} = \sqrt{\bar{\alpha}_{t-1}} \hat{\mathbf{x}}_c^\omega(\mathbf{x}_t) + \sqrt{1 - \bar{\alpha}_{t-1}} \hat{\epsilon}_c^\omega(\mathbf{x}_t)$ 5: end for 6: return \mathbf{x}_0	Require: $\mathbf{x}_T \sim \mathcal{N}(0, \mathbf{I}_d)$, $\lambda \in [0, 1]$ 1: for $i = T$ to 1 do 2: $\hat{\epsilon}_c^\lambda(\mathbf{x}_t) = \hat{\epsilon}_\emptyset(\mathbf{x}_t) + \lambda[\epsilon_c(\mathbf{x}_t) - \hat{\epsilon}_\emptyset(\mathbf{x}_t)]$ 3: $\hat{\mathbf{x}}_c^\lambda(\mathbf{x}_t) \leftarrow (\mathbf{x}_t - \sqrt{1 - \bar{\alpha}_t} \hat{\epsilon}_c^\lambda(\mathbf{x}_t)) / \sqrt{\bar{\alpha}_t}$ 4: $\mathbf{x}_{t-1} = \sqrt{\bar{\alpha}_{t-1}} \hat{\mathbf{x}}_c^\lambda(\mathbf{x}_t) + \sqrt{1 - \bar{\alpha}_{t-1}} \hat{\epsilon}_\emptyset(\mathbf{x}_t)$ 5: end for 6: return \mathbf{x}_0

Figure 2: Comparison between reverse diffusion process by CFG and CFG++. CFG++ propose a simple but surprisingly effective fix: using $\hat{\epsilon}_\emptyset(\mathbf{x}_t)$ instead of $\hat{\epsilon}_c^\omega(\mathbf{x}_t)$ in updating \mathbf{x}_{t-1} .

is invertible up to the discretization error, simplifying image editing. Comparing CFG++ against CFG shows that we achieve consistently better sample quality for text-to-image (T2I) generation, significantly better DDIM inversion capabilities that lead to enhanced reconstruction and editing, and enabling the incorporation of CFG guidance to diffusion inverse solvers (DIS) (Chung et al., 2023a). While the applications of CFG++ that we show in this work are limited, we believe that our work will have a broad impact that can be applied to all applications that leverage text guidance through the traditional CFG.

2 BACKGROUND

Diffusion models. Diffusion models (Ho et al., 2020; Song et al., 2021b; Karras et al., 2022) are generative models designed to learn the reversal of a forward noising process. This process starts with an initial distribution $p_0(\mathbf{x})$ where $\mathbf{x} \in \mathbb{R}^n$, and progresses towards the standard Gaussian distribution $p_T(\mathbf{x}) \approx \mathcal{N}(\mathbf{0}, \mathbf{I})$, utilizing forward Gaussian perturbation kernels. Sampling from the data distribution can be performed by solving either the reverse stochastic differential equation (SDE) or the equivalent probability-flow ordinary differential equation (PF-ODE) (Song et al., 2021b). For example, under the choice $p(\mathbf{x}_t | \mathbf{x}_0) = \mathcal{N}(\mathbf{x}_0, t^2 \mathbf{I})$, the generative PF-ODE reads

$$d\mathbf{x}_t = -t \nabla_{\mathbf{x}_t} \log p(\mathbf{x}_t) dt = \frac{\mathbf{x}_t - \mathbb{E}[\mathbf{x}_0 | \mathbf{x}_t]}{t} dt, \quad \mathbf{x}_T \sim p_T(\mathbf{x}_T), \quad (1)$$

where Tweedie’s formula (Efron, 2011) $\mathbb{E}[\mathbf{x}_0 | \mathbf{x}_t] = \mathbf{x}_t + t^2 \nabla_{\mathbf{x}_t} \log p(\mathbf{x}_t)$ is applied to achieve the second equality. Thus, the score function $\nabla_{\mathbf{x}_t} \log p(\mathbf{x}_t)$ plays the key role in diffusion models. One can approximate an equivalent parameterization of the score function via denoising score matching (Hyvärinen & Dayan, 2005) or epsilon-matching (Ho et al., 2020), etc. When aiming for a text-conditional diffusion model that can condition on arbitrary \mathbf{c} , one can extend epsilon matching to a conditional one as:

$$\min_{\theta} \mathbb{E}_{\mathbf{x}_t \sim p(\mathbf{x}_t | \mathbf{x}_0), \{\mathbf{x}_0, \mathbf{c}\} \sim p(\mathbf{x}_0, \mathbf{c}), \boldsymbol{\epsilon} \sim \mathcal{N}(0, \mathbf{I})} [\|\boldsymbol{\epsilon}_\theta(\mathbf{x}_t, \mathbf{c}) - \boldsymbol{\epsilon}\|_2^2], \quad (2)$$

where the condition is dropped with a certain probability (Ho & Salimans, 2021) so that null conditioning with $\mathbf{c} = \emptyset$ is possible. The neural network architecture of $\boldsymbol{\epsilon}_\theta$ is designed so that the condition \mathbf{c} can *modulate* the output through cross attention (Rombach et al., 2022). For simplicity in notation throughout the paper, we define $\hat{\epsilon}_c := \boldsymbol{\epsilon}_\theta(\mathbf{x}_t, \mathbf{c})$ and $\hat{\epsilon}_\emptyset := \boldsymbol{\epsilon}_\theta(\mathbf{x}_t, \emptyset)$ by dropping θ and \mathbf{x}_t .

Extending the result of the Tweedie’s formula to the unconditional case under the variance preserving (VP) framework of DDPMs (Ho et al., 2020), we have

$$\mathbb{E}[\mathbf{x}_0 | \mathbf{x}_t, \emptyset] = \hat{\mathbf{x}}_\emptyset(\mathbf{x}_t) := (\mathbf{x}_t - \sqrt{1 - \bar{\alpha}_t} \hat{\epsilon}_\emptyset(\mathbf{x}_t)) / \sqrt{\bar{\alpha}_t}. \quad (3)$$

Leveraging (3), it is common to use DDIM sampling (Song et al., 2021b) to solve the conditional probability-flow ODE (PF-ODE) of the generative process. Specifically, a single iteration reads

$$\hat{\mathbf{x}}_\emptyset = (\mathbf{x}_t - \sqrt{1 - \bar{\alpha}_t} \hat{\epsilon}_\emptyset) / \sqrt{\bar{\alpha}_t} \quad (4)$$

$$\mathbf{x}_{t-1} = \sqrt{\bar{\alpha}_{t-1}} \hat{\mathbf{x}}_\emptyset + \sqrt{1 - \bar{\alpha}_{t-1}} \hat{\epsilon}_\emptyset, \quad (5)$$

where $\hat{\mathbf{x}}_\emptyset := \hat{\mathbf{x}}_\emptyset(\mathbf{x}_t) = \mathbb{E}[\mathbf{x}_0 | \mathbf{x}_t, \emptyset]$ is the denoised signal by Tweedie’s formula, and (5) corresponds to the *renoiseing* step. This is repeated for $t = T, T-1, \dots, 1$.

For modern diffusion models, it is common to train a diffusion model in the latent space (Rombach et al., 2022) with the latent variable \mathbf{z} . While most of our experiments are performed with latent

diffusion models (LDM), as our framework holds both for pixel- and latent- diffusion models, we will simply use the notation \mathbf{x} regardless of the choice.

Classifier free guidance. For a conditional diffusion, Ho & Salimans (2021) considered the sharpened posterior distribution $p^\omega(\mathbf{x}|\mathbf{c}) \propto p(\mathbf{x})p(\mathbf{c}|\mathbf{x})^\omega$. Using Bayes rule for some timestep t ,

$$\nabla_{\mathbf{x}} \log p^\omega(\mathbf{x}_t|\mathbf{c}) = \nabla_{\mathbf{x}_t} \log p(\mathbf{x}_t) + \omega(\nabla_{\mathbf{x}_t} \log p(\mathbf{x}_t|\mathbf{c}) - \nabla_{\mathbf{x}_t} \log p(\mathbf{x}_t)) \quad (6)$$

Parametrizing the score function with ϵ_θ , as in DDPM (Ho et al., 2020), we have

$$\hat{\epsilon}_c^\omega(\mathbf{x}_t) := \hat{\epsilon}_\emptyset(\mathbf{x}_t) + \omega[\hat{\epsilon}_c(\mathbf{x}_t) - \hat{\epsilon}_\emptyset(\mathbf{x}_t)] \quad (7)$$

where we introduce a compact notation $\hat{\epsilon}_c^\omega$ that guides the sampling from the sharpened posterior. When sampling with CFG guidance with DDIM sampling, one replaces $\hat{\epsilon}_\emptyset$ with $\hat{\epsilon}_c^\omega$ for both the Tweedie estimate (4) and the subsequent update step (5), leading to Algorithm 1.

Diffusion model-based inverse problem solvers. Diffusion model-based inverse problem solvers (DIS) aim to perform posterior sampling from an unconditional diffusion model (Kadkhodaie & Simoncelli, 2021; Chung et al., 2023a; Song et al., 2023a; Kim et al., 2024). Specifically, for a given loss function $\ell(\mathbf{x})$ which often stems from the likelihood for measurement consistency¹, the goal of DIS is to address the following optimization problem

$$\min_{\mathbf{x} \in \mathcal{M}} \ell(\mathbf{x}) \quad (8)$$

where \mathcal{M} represents the clean data manifold sampled from unconditional distribution $p_0(\mathbf{x})$. Consequently, it is essential to navigate in a way that minimizes cost while also identifying the correct clean manifold.

Recently, Chung et al. (2023a) proposed a general technique called diffusion posterior sampling (DPS), where the updated estimate from the noisy sample $\mathbf{x}_t \in \mathcal{M}_t$ is constrained to stay on the same noisy manifold \mathcal{M}_t . This is achieved by computing the manifold constrained gradient (MCG) (Chung et al., 2022) on a noisy sample $\mathbf{x}_t \in \mathcal{M}_t$ as $\nabla_{\mathbf{x}_t}^{mcg} \ell(\mathbf{x}_t) := \nabla_{\mathbf{x}_t} \ell(\hat{\mathbf{x}}_t)$, where $\hat{\mathbf{x}}_t$ is the denoised sample in (3) through Tweedie's formula. The resulting algorithm can be stated as follows:

$$\mathbf{x}_{t-1} = \sqrt{\bar{\alpha}_{t-1}} (\hat{\mathbf{x}}_\emptyset - \gamma_t \nabla_{\mathbf{x}_t} \ell(\hat{\mathbf{x}}_\emptyset)) + \sqrt{1 - \bar{\alpha}_{t-1}} \hat{\epsilon}_\emptyset, \quad (9)$$

where $\gamma_t > 0$ denotes the step size. Under the linear manifold assumption (Chung et al., 2022; 2023a), this allows precise transition to \mathcal{M}_{t-1} . Therefore, by performing (9) from $t = T$ to $t = 0$, we can solve the optimization problem (8) with $\mathbf{x}_0 \in \mathcal{M}$. Unfortunately, the computation of MCG requires computationally expensive backpropagation and is often unstable (Poole et al., 2022; Du et al., 2023).

In another work, Chung et al. (2024) shows that (9) can be equivalently represented as

$$\mathbf{x}_{t-1} = \sqrt{\bar{\alpha}_{t-1}} P_{\mathcal{M}} (\hat{\mathbf{x}}_\emptyset - \gamma_t \nabla_{\hat{\mathbf{x}}_\emptyset} \ell(\hat{\mathbf{x}}_\emptyset)) + \sqrt{1 - \bar{\alpha}_{t-1}} \hat{\epsilon}_\emptyset, \quad (10)$$

where $P_{\mathcal{M}}$ denotes the projection on the clean manifold \mathcal{M} . This implies that the data consistency update step becomes a standard gradient step, followed by the projection on the clean manifold. Importantly, under the commonly used linear manifold assumption in DPS, the one step update by $\hat{\mathbf{x}}_\emptyset - \gamma_t \nabla_{\hat{\mathbf{x}}_\emptyset} \ell(\hat{\mathbf{x}}_\emptyset)$ or multi-step update employing the conjugate gradient (CG) method are guaranteed to remain within a linear subspace, thus obviating the need for explicit computation of $P_{\mathcal{M}}$, i.e.

$$\mathbf{x}_{t-1} \simeq \sqrt{\bar{\alpha}_{t-1}} (\hat{\mathbf{x}}_\emptyset - \gamma_t \nabla_{\hat{\mathbf{x}}_\emptyset} \ell(\hat{\mathbf{x}}_\emptyset)) + \sqrt{1 - \bar{\alpha}_{t-1}} \hat{\epsilon}_\emptyset. \quad (11)$$

This method, often referred to as the decomposed diffusion sampling (DDS), bypasses the computation of the score Jacobian, similar to Poole et al. (2022), making it stable and suitable for large scale medical imaging inverse problems (Chung et al., 2024). In the following, we leverage the insight from DDS to propose an algorithm to improve upon the CFG algorithm.

¹For example, for a given measurement model $\mathbf{y} = A\mathbf{x} + \mathbf{w}$ with $\mathbf{w} \sim \mathcal{N}(\mathbf{x}_0, \sigma^2 \mathbf{I})$, the loss function is the data consistency (DC) loss given by $\ell(\mathbf{x}) = \|\mathbf{y} - A\mathbf{x}\|^2 / 2\sigma^2$.

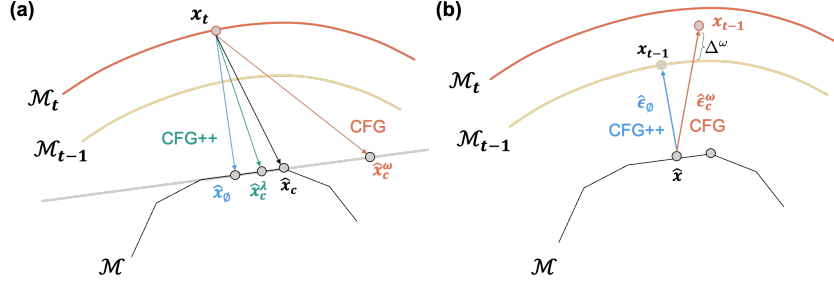


Figure 3: Off-manifold phenomenon of CFG arise from: (a) the typical CFG scale $\omega > 1.0$ which leads to extrapolation and deviation from the piecewise linear data manifold, and (b) CFG's renoising process, which introduces a nonzero offset from the correct manifold. CFG++ effectively mitigates all these artifacts.

3 CFG++ : MANIFOLD-CONSTRAINED CFG

3.1 DERIVATION OF CFG++

Instead of uncritically adopting the sharpened posterior distribution $p^\omega(\mathbf{x}|\mathbf{c}) \propto p(\mathbf{x})p(\mathbf{c}|\mathbf{x})^\omega$ as introduced by Ho & Salimans (2021) and further explored in the Bayesian CFG formulation, we adopt a fundamentally different strategy by reformulating text-guidance as an optimization problem. Specifically, our focus is on identifying a loss function $\ell(\mathbf{x})$ in (8) such that, when minimized under the condition set by the text, enables the reverse diffusion process to progressively generate samples that increasingly satisfy the text condition.

One of the most significant contributions of this paper is to reveal that the text-conditioned score matching loss or score distillation sampling (SDS) loss is also ideally suited for our purpose. Specifically, we are interested in solving the following inverse problem through diffusion models:

$$\min_{\mathbf{x} \in \mathcal{M}} \ell_{sds}(\mathbf{x}), \quad \ell_{sds}(\mathbf{x}) := \|\epsilon_\theta(\sqrt{\bar{\alpha}_t}\mathbf{x} + \sqrt{1-\bar{\alpha}_t}\epsilon, \mathbf{c}) - \epsilon\|_2^2 \quad (12)$$

This implies that our goal is to identify solutions on the clean manifold \mathcal{M} that optimally align with the text condition \mathbf{c} .

To avoid the Jacobian computation, in this paper we attempt to solve (12) through decomposed diffusion sampling (DDS). The resulting sampling process from reverse diffusion is then given by

$$\mathbf{x}_{t-1} = \sqrt{\bar{\alpha}_{t-1}} (\hat{\mathbf{x}}_\phi - \gamma_t \nabla_{\hat{\mathbf{x}}_\phi} \ell_{sds}(\hat{\mathbf{x}}_\phi)) + \sqrt{1-\bar{\alpha}_{t-1}} \hat{\epsilon}_\phi \quad (13)$$

which is analogous to (11). Consequently, the remaining technical issue is to compute $\nabla_{\hat{\mathbf{x}}_\phi} \ell_{sds}(\hat{\mathbf{x}}_\phi)$. To answer this, by using the forward diffusion to generate $\mathbf{x}_t = \sqrt{\bar{\alpha}_t}\mathbf{x} + \sqrt{1-\bar{\alpha}_t}\epsilon$ from the clean image $\mathbf{x} \in \mathcal{M}$, we convert the objective function in (12) into the following equivalent loss:

$$\ell_{sds}(\mathbf{x}) = \|\epsilon - \epsilon_\theta(\mathbf{x}_t, \mathbf{c})\|^2 = \left\| \frac{\mathbf{x}_t - \sqrt{\bar{\alpha}_t}\mathbf{x}}{\sqrt{1-\bar{\alpha}_t}} - \frac{\mathbf{x}_t - \sqrt{\bar{\alpha}_t}\hat{\mathbf{x}}_\phi}{\sqrt{1-\bar{\alpha}_t}} \right\|^2 \quad (14)$$

$$= \frac{\bar{\alpha}_t}{1-\bar{\alpha}_t} \|\mathbf{x} - \hat{\mathbf{x}}_\phi\|^2 \quad (15)$$

where we use the conditional Tweedie formula derived by replacing $\hat{\epsilon}_\phi$ in (4) by the conditioned score $\hat{\epsilon}_c$. Similar observation has been made in DreamSampler (Kim et al., 2024) and HiFA (Zhu et al., 2023). Consequently, $\nabla_{\hat{\mathbf{x}}_\phi} \ell_{sds}(\hat{\mathbf{x}}_\phi)$ can be readily computable and the resulting DDS sampling process can be simplified as

$$\mathbf{x}_{t-1} = \sqrt{\bar{\alpha}_{t-1}} (\hat{\mathbf{x}}_\phi + \lambda(\hat{\mathbf{x}}_\phi - \hat{\mathbf{x}}_\phi)) + \sqrt{1-\bar{\alpha}_{t-1}} \hat{\epsilon}_\phi \quad (16)$$

where $\lambda := \frac{2\bar{\alpha}_t}{1-\bar{\alpha}_t} \gamma_t$. Although concise, (16) can be further simplified to a similar form of the traditional CFG as described in Algorithm 1. Specifically, note that

$$\hat{\mathbf{x}}_\phi + \lambda(\hat{\mathbf{x}}_\phi - \hat{\mathbf{x}}_\phi) = (\mathbf{x}_t - \sqrt{1-\bar{\alpha}_t} \hat{\epsilon}_c^\lambda(\mathbf{x}_t)) / \sqrt{\bar{\alpha}_t} \quad (17)$$

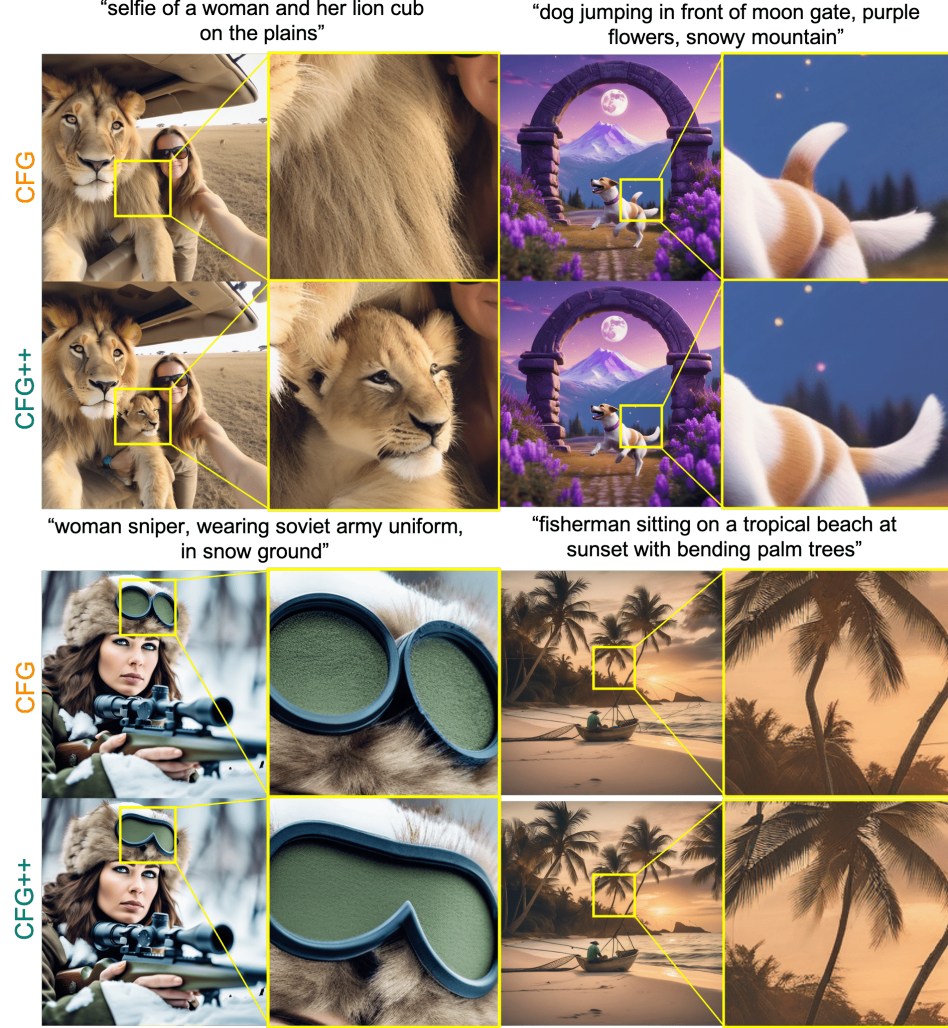


Figure 4: Enhanced T2I results by SDXL ($\omega = 9.0$, $\lambda = 0.8$) with CFG++. Under CFG, the lion cub is not visible (top-left), the dog appears with two tails (top-right), the goggles have an unusual shape (bottom-left), and the tree trunk is folded (bottom-right). These artifacts are absent in those produced by CFG++.

where

$$\hat{\epsilon}_c^\lambda(\mathbf{x}_t) := \hat{\epsilon}_\emptyset(\mathbf{x}_t) + \lambda[\hat{\epsilon}_c(\mathbf{x}_t) - \hat{\epsilon}_\emptyset(\mathbf{x}_t)] \quad (18)$$

Therefore, (16) can be equivalently represented by:

$$\hat{\mathbf{x}}_c^\lambda(\mathbf{x}_t) = (\mathbf{x}_t - \sqrt{1 - \bar{\alpha}_t} \hat{\epsilon}_c^\lambda(\mathbf{x}_t)) / \sqrt{\bar{\alpha}_t} \quad (19)$$

$$\mathbf{x}_{t-1} = \sqrt{\bar{\alpha}_{t-1}} \hat{\mathbf{x}}_c^\lambda(\mathbf{x}_t) + \sqrt{1 - \bar{\alpha}_{t-1}} \hat{\epsilon}_\emptyset(\mathbf{x}_t) \quad (20)$$

which is summarized in Algorithm 2.

By examining Algorithm 1 and Algorithm 2, we observe a notable similarity between CFG and CFG++. However, a crucial difference exists. Specifically, in CFG++, the renoising process after applying Tweedie's formula should utilize the unconditional noise $\hat{\epsilon}_\emptyset(\mathbf{x}_t)$ instead of $\hat{\epsilon}_c^\omega(\mathbf{x}_t)$. This surprisingly simple fix to the original CFG algorithm leads to smoother trajectory of generation, (Fig. 1 bottom) and generation with superior quality (Fig. 1 top). Moreover, CFG++ can also be easily extended to significantly improve DDIM inversion, which is known to be prone to failure by standard CFG (Mokady et al., 2023). See Fig. 1 (middle) for representative results and Sec. 4.2 for further discussions. In the following section, we present a theoretical analysis of CFG++ to investigate the origin of this improvement.

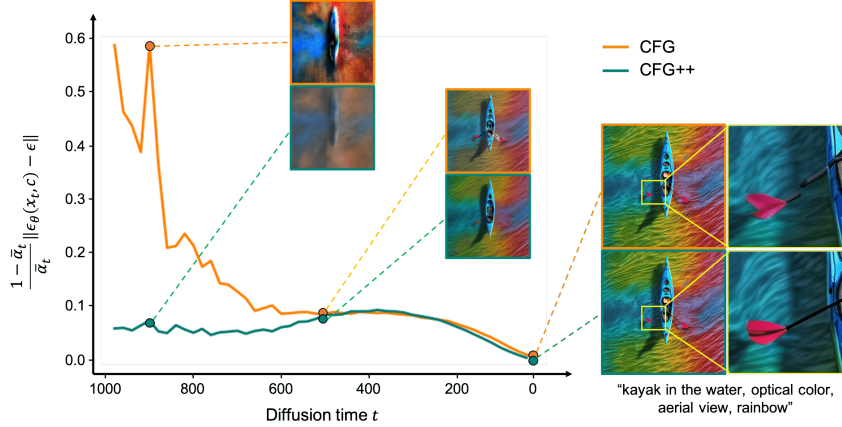


Figure 5: The normalized text-conditioned score matching loss throughout the reverse diffusion process for both CFG and CFG++.

3.2 GEOMETRY OF CFG++

Mitigating off-manifold phenomenon. In Fig. 1 (bottom), we illustrate the evolution of the posterior mean through Tweedie’s formula during the reverse diffusion process. Notably, in the early phases of reverse diffusion sampling under CFG, there is a sudden shift in the image and intense color saturation, followed by only minor changes until later stages. This abrupt transition in the posterior mean is somewhat unexpected, as the reverse diffusion process is designed to progressively refine resolution, moving from a noisier to a clearer manifold. Similar phenomena are depicted in Fig. 13 in Appendix. We refer to this as the *off-manifold* phenomenon, which will be clarified shortly. Conversely, under CFG++, the posterior mean evolves gradually, transitioning smoothly from a low-resolution image to high-resolution details. This indicates that CFG++ is less prone to the off-manifold phenomenon observed with CFG. In the following, we provide a theoretical analysis of the origin of the off-manifold phenomenon and explain why CFG++ can mitigate this issue.

By examining (16) and (19) as well as CFG in Algorithm 1, we can easily see that the Tweedie’s formula for the CFG++ and CFG can be equivalently represented by

$$\hat{x}_c^\lambda(\mathbf{x}_t) = (1 - \lambda)\hat{x}_\emptyset(\mathbf{x}_t) + \lambda\hat{x}_c(\mathbf{x}_t), \quad \hat{x}_c^\omega(\mathbf{x}_t) = (1 - \omega)\hat{x}_\emptyset(\mathbf{x}_t) + \omega\hat{x}_c(\mathbf{x}_t) \quad (21)$$

This implies that $\lambda, \omega \in [0, 1]$ facilitates an *interpolation* between the unconditional and the conditional posterior means. However, given the typical CFG scale $\omega > 1.0$, we observe that CFG *extrapolates* beyond the unconditional and the conditional posterior means established by Tweedie’s formula. Consequently, under the usual assumption that the clean manifold to be piecewise linear around the posterior mean derived via Tweedie’s formula, the conditional posterior mean estimates from traditional CFG, obtained with a guidance scale outside the range of $[0, 1]$, can extend beyond the piecewise linear manifold. This may lead to the estimates potentially ‘falling off’ the data manifold, as depicted by an orange arrow pointing downwards in Fig. 3(a). We conjecture that this is one of the primary contributors to the off-manifold phenomenon. Thus, we select $\lambda \in [0, 1]$ as the guidance scale for CFG++ to ensure it remains an *interpolation* between the unconditional and conditional Tweedie, thus preventing it from ‘falling off’ the clean data manifold.

An additional source of the off-manifold phenomenon in CFG occurs during the transition from the clean manifold \mathcal{M} to the subsequent noisy manifold \mathcal{M}_{t-1} . Specifically, even from the same point in the clean manifold, the use of $\hat{\epsilon}_c^\omega(\mathbf{x}_t)$ for this transition introduces a nonzero offset $\Delta^\omega := \omega\sqrt{1 - \bar{\alpha}_{t-1}}(\hat{\epsilon}_c(\mathbf{x}_t) - \hat{\epsilon}_\emptyset(\mathbf{x}_t))$ from \mathcal{M}_{t-1} , as illustrated in Fig. 3 (b). This leads to the invalid lifts from \mathcal{M} to \mathcal{M}_{t-1} . On the other hand, we note that the renoising process of CFG++ follows the standard DDIM, resulting in the accurate transition to \mathcal{M}_{t-1} .

Text-Image alignment. In Fig. 1 (top), we display images generated by SDXL using the prompt “Kayak in the water, optical color, areal view, rainbow”. The generated image on the left is guided by the traditional CFG, while the one on the right is produced with our CFG++. Although both images look impressive and appear to align well with the given text prompt, a closer examination reveals a

Algorithm 3 DDIM Inversion with CFG	Algorithm 4 DDIM Inversion with CFG++
Require: $\mathbf{x}_0, 0 \leq \omega \in \mathbb{R}$ 1: for $i = 0$ to $T - 1$ do 2: $\hat{\epsilon}_c^\omega(\mathbf{x}_t) = \hat{\epsilon}_\emptyset(\mathbf{x}_t) + \omega[\hat{\epsilon}_c(\mathbf{x}_t) - \hat{\epsilon}_\emptyset(\mathbf{x}_t)]$ 3: $\hat{\mathbf{x}}_c^\omega(\mathbf{x}_t) \leftarrow (\mathbf{x}_t - \sqrt{1 - \bar{\alpha}_t} \hat{\epsilon}_c^\omega(\mathbf{x}_t)) / \sqrt{\bar{\alpha}_t}$ 4: $\mathbf{x}_{t+1} = \sqrt{\bar{\alpha}_{t+1}} \hat{\mathbf{x}}_c^\omega(\mathbf{x}_t) + \sqrt{1 - \bar{\alpha}_{t+1}} \hat{\epsilon}_c^\omega(\mathbf{x}_t)$ 5: end for 6: return \mathbf{x}_T	Require: $\mathbf{x}_0, \lambda \in [0, 1]$ 1: for $i = 0$ to $T - 1$ do 2: $\hat{\epsilon}_c^\lambda(\mathbf{x}_t) = \hat{\epsilon}_\emptyset(\mathbf{x}_t) + \lambda[\hat{\epsilon}_c(\mathbf{x}_t) - \hat{\epsilon}_\emptyset(\mathbf{x}_t)]$ 3: $\hat{\mathbf{x}}_c^\lambda(\mathbf{x}_t) \leftarrow (\mathbf{x}_t - \sqrt{1 - \bar{\alpha}_t} \hat{\epsilon}_\emptyset(\mathbf{x}_t)) / \sqrt{\bar{\alpha}_t}$ 4: $\mathbf{x}_{t+1} = \sqrt{\bar{\alpha}_{t+1}} \hat{\mathbf{x}}_c^\lambda(\mathbf{x}_t) + \sqrt{1 - \bar{\alpha}_{t+1}} \hat{\epsilon}_c^\lambda(\mathbf{x}_t)$ 5: end for 6: return \mathbf{x}_T

Figure 6: Comparison between DDIM inversion. CFG++ propose a simple yet effective fix: using $\hat{\epsilon}_\emptyset(\mathbf{x}_t)$ instead of $\hat{\epsilon}_c^\omega(\mathbf{x}_t)$ in Tweedie’s denoising step.

significant difference. For instance, one of the oars in the CFG-guided image is broken in the middle, which shows a misalignment with the text prompt. This type of artifact is substantially reduced in the CFG++ version, where the oars are depicted intact. The examples provided by SDXL in Fig. 4 further demonstrate the enhanced text-to-image alignment achieved with CFG++. For instance, the lion cub is not visible in Fig. 4(top-left), the dog appears with two tails in Fig. 4(top-right), the goggles have an unusual shape in Fig. 4(bottom-left), and the tree trunk is folded in Fig. 4(bottom-right). These artifacts, observed in the images generated by CFG, are absent in those produced by CFG++.

In fact, this enhanced alignment capability is a natural consequence of CFG++, which directly minimizes the text-conditioned score-matching loss as shown in (12). In contrast, CFG indirectly seeks text alignment through the sharpened posterior distribution $p^\omega(\mathbf{x}|c) \propto p(\mathbf{x})p(c|\mathbf{x})^\omega$. Therefore, CFG++ inherently outperform CFG in terms of text alignment due to its fundamental design principle. For example, Fig. 5 displays the normalized text-conditioned score matching loss, represented as $(1 - \bar{\alpha}_t) \|\epsilon - \epsilon_\theta(\mathbf{x}_t, c)\|^2 / \bar{\alpha}_t = \|\mathbf{x} - \hat{\mathbf{x}}_c\|^2$, throughout the reverse diffusion sampling process for both CFG and CFG++. The loss plot associated with CFG shows fluctuations and maintains a noticeable gap compared to CFG++ even after the completion of the reverse diffusion process. In fact, the fluctuation associated with CFG is also related to the off-manifold issue, and from Fig. 5 we can easily see that the off-manifold phenomenon is more dominant at early stage of reverse diffusion sampling. Conversely, the loss trajectory for CFG++ demonstrates a much smoother variation, particularly during the early stages of reverse diffusion.

DDIM inversion. As discussed in (Song et al., 2021a), the denoising process for unconditional DDIM is approximately invertible, meaning that \mathbf{x}_t can generally be recovered from \mathbf{x}_{t-1} . Specifically, from (4) and (5), we have the following approximate inversion formula for unconditional DDIM:

$$\begin{aligned}\hat{\mathbf{x}}_\emptyset(\mathbf{x}_t) &= (\mathbf{x}_{t-1} - \sqrt{1 - \bar{\alpha}_{t-1}} \hat{\epsilon}_\emptyset(\mathbf{x}_t)) / \sqrt{\bar{\alpha}_{t-1}} \\ &\simeq (\mathbf{x}_{t-1} - \sqrt{1 - \bar{\alpha}_{t-1}} \hat{\epsilon}_\emptyset(\mathbf{x}_{t-1})) / \sqrt{\bar{\alpha}_{t-1}}\end{aligned}\quad (22)$$

$$\begin{aligned}\mathbf{x}_t &= \sqrt{\bar{\alpha}_t} \hat{\mathbf{x}}_\emptyset(\mathbf{x}_t) + \sqrt{1 - \bar{\alpha}_t} \hat{\epsilon}_\emptyset(\mathbf{x}_t) \\ &\simeq \sqrt{\bar{\alpha}_t} \hat{\mathbf{x}}_\emptyset(\mathbf{x}_t) + \sqrt{1 - \bar{\alpha}_t} \hat{\epsilon}_\emptyset(\mathbf{x}_{t-1})\end{aligned}\quad (23)$$

where the approximation arises from $\hat{\epsilon}_\emptyset(\mathbf{x}_t) \simeq \hat{\epsilon}_\emptyset(\mathbf{x}_{t-1})$. By assuming $\hat{\epsilon}_c^\omega(\mathbf{x}_t) \simeq \hat{\epsilon}_c^\omega(\mathbf{x}_{t-1})$, a similar inversion procedure has been employed for conditional DDIM inversion under CFG, by replacing $\hat{\epsilon}_\emptyset$ by $\hat{\epsilon}_c^\omega$ as detailed in Algorithm 3.

On the other hand, by examining (19) and (20), we can obtain the approximate DDIM inversion formula under CFG++:

$$\hat{\mathbf{x}}_c^\lambda(\mathbf{x}_t) \simeq (\mathbf{x}_{t-1} - \sqrt{1 - \bar{\alpha}_{t-1}} \hat{\epsilon}_\emptyset(\mathbf{x}_{t-1})) / \sqrt{\bar{\alpha}_{t-1}} \quad (24)$$

$$\mathbf{x}_t \simeq \sqrt{\bar{\alpha}_t} \hat{\mathbf{x}}_c^\lambda(\mathbf{x}_t) + \sqrt{1 - \bar{\alpha}_t} \hat{\epsilon}_c^\lambda(\mathbf{x}_{t-1}) \quad (25)$$

where we apply the approximation $\hat{\epsilon}_c^\lambda(\mathbf{x}_t) \simeq \hat{\epsilon}_c^\lambda(\mathbf{x}_{t-1})$ alongside the usual assumption $\hat{\epsilon}_\emptyset(\mathbf{x}_t) \simeq \hat{\epsilon}_\emptyset(\mathbf{x}_{t-1})$. This formulation underpins the CFG++ guided DDIM inversion algorithm, presented in Algorithm 4.

In practice, the error $\hat{\epsilon}_\emptyset(\mathbf{x}_t) \simeq \hat{\epsilon}_\emptyset(\mathbf{x}_{t-1})$ is relatively small, so the unconditional DDIM inversion by (22) and (23) lead to relatively insignificant errors. Unfortunately, the corresponding inversion from conditional diffusion under CFG is quite distorted as noted in (Mokady et al., 2023; Wallace et al., 2023). In fact, this distortion is originated from the inaccuracy of the approximation $\hat{\epsilon}_c^\omega(\mathbf{x}_t) \simeq \hat{\epsilon}_c^\omega(\mathbf{x}_{t-1})$. More specifically, even when $\hat{\epsilon}_\emptyset(\mathbf{x}_t) \simeq \hat{\epsilon}_\emptyset(\mathbf{x}_{t-1})$, the approximation error from the CFG

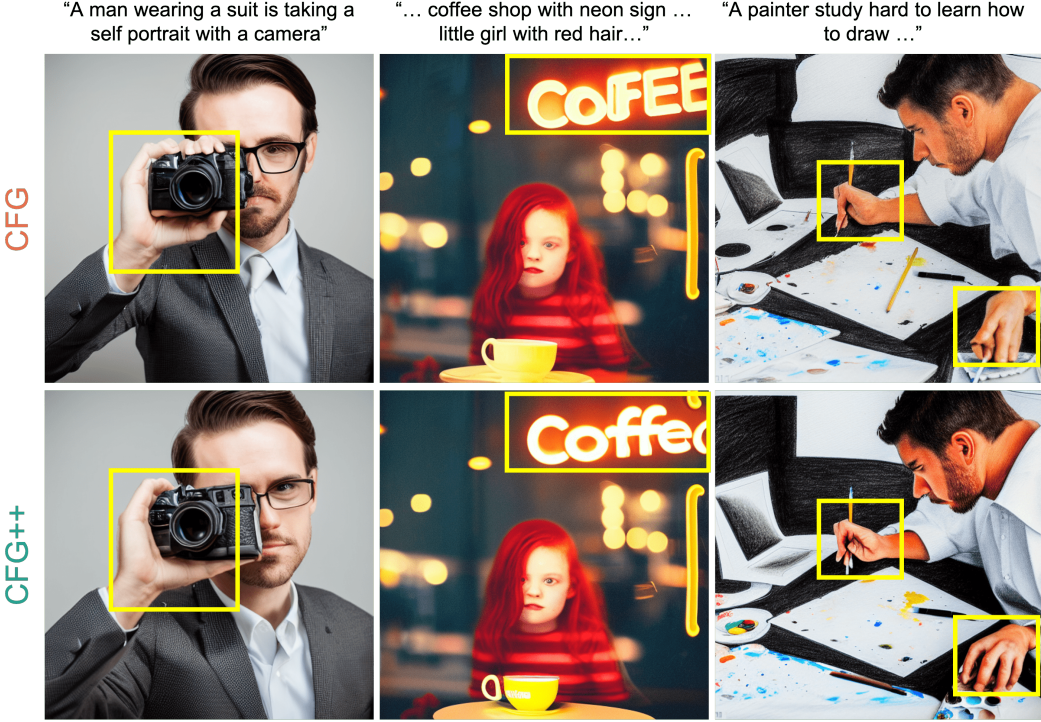


Figure 7: T2I using SD v1.5, CFG vs CFG++ ($\omega = 9.0, \lambda = 0.8$). Unnatural depictions of human hands, and incorrect renderings of the text by CFG are corrected in CFG++

Method	$\omega = 2.0, \lambda = 0.2$		$\omega = 5.0, \lambda = 0.4$		$\omega = 7.5, \lambda = 0.6$		$\omega = 9.0, \lambda = 0.8$		$\omega = 12.5, \lambda = 1.0$	
	FID \downarrow	CLIP \uparrow	FID \downarrow	CLIP \downarrow	FID \downarrow	CLIP \uparrow	FID \downarrow	CLIP \uparrow	FID \downarrow	CLIP \uparrow
CFG (Ho & Salimans, 2021)	13.84	0.298	15.08	0.310	17.71	0.312	20.01	0.312	21.23	0.313
CFG++ (ours)	12.75	0.303	14.95	0.310	17.47	0.312	19.34	0.313	20.88	0.313

Table 1: Quantitative evaluation (FID, CLIP-similarity) of T2I with SD v1.5

is given by

$$\begin{aligned} \epsilon_{cfg} := \hat{\epsilon}_c^\omega(\mathbf{x}_t) - \hat{\epsilon}_c^\omega(\mathbf{x}_{t-1}) &= (\hat{\epsilon}_\phi(\mathbf{x}_t) - \hat{\epsilon}_\phi(\mathbf{x}_{t-1})) + \omega(d\hat{\epsilon}_c(\mathbf{x}_t) - d\hat{\epsilon}_c(\mathbf{x}_{t-1})) \\ &\simeq \omega(d\hat{\epsilon}_c(\mathbf{x}_t) - d\hat{\epsilon}_c(\mathbf{x}_{t-1})), \end{aligned} \quad (26)$$

where $d\hat{\epsilon}_c(\mathbf{x}_t) := \hat{\epsilon}_c(\mathbf{x}_t) - \hat{\epsilon}_\phi(\mathbf{x}_t)$. Note that this error becomes significant for high guidance scale ω . Accordingly, the guidance scale must be heavily downweighted in order for inversions on real world images to be stable, thus limiting the strength of edits. To mitigate this issue, the authors in (Mokady et al., 2023; Wallace et al., 2023) developed null text optimization and coupled transform techniques, respectively.

On the other hand, under the usual DDIM assumption $\hat{\epsilon}_\phi(\mathbf{x}_t) \simeq \hat{\epsilon}_\phi(\mathbf{x}_{t-1})$, the approximation error of CFG++ mainly arises from (25), which is smaller than that of CFG since we have

$$\|\epsilon_{cfg++}\| = \lambda \|d\hat{\epsilon}_c(\mathbf{x}_t) - d\hat{\epsilon}_c(\mathbf{x}_{t-1})\| < \|\epsilon_{cfg}\| \quad (27)$$

thanks to $\lambda < \omega$. Therefore, CFG++ significantly improves the DDIM inversion as shown Fig. 1 (middle) for representative results and Sec. 4.2 for further discussions.

4 EXPERIMENTAL RESULTS

In this section, we design experiments to show the limitation of CFG and how CFG++ can effectively mitigate these downsides. We select Stable Diffusion (Rombach et al., 2022) (SD) as our baseline model for its widespread use. Experiments are conducted using SD v1.5 from diffusers (Patil et al.,

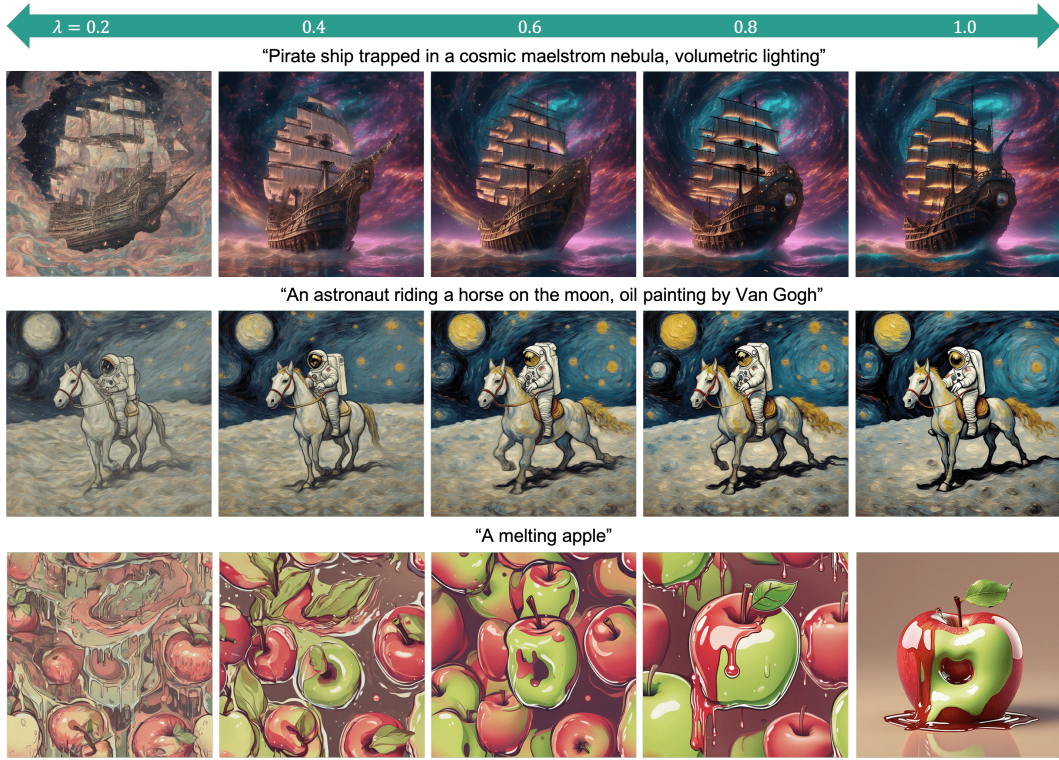


Figure 8: Guidance scale interpolation of T2I using SDXL with CFG++. The generated visuals align more significantly with the given textual description as the guidance scale increase to 1.

2022) unless specified otherwise. Notice that we use the conditioning scale $\lambda \in [0, 1]$ for CFG++ whereas for standard CFG, the typical range is $\omega > 1.0$. When searching for the matched guidance values of ω and λ for a fair comparison, we fix $\lambda = 0.2, 0.4, 0.6, 0.8, 1.0$ and find the ω values that produce the images that are of closest proximity in terms of LPIPS distance given the same seed. We found that the corresponding values were $\omega = 2.0, 5.0, 7.5, 9.0, 12.5$, respectively, as shown in appendix Fig. 17.

4.1 TEXT-TO-IMAGE GENERATION

Using the corresponding scales for ω and λ , we directly compare the performance of the T2I task using SD v1.5 and SDXL. In Tab. 1, we observe a constant improvement of the FID metric across all guidance scales, with approximately the same level of CLIP similarity or better. The improvements can also be clearly seen in Fig. 7 (SD v1.5), where the unnatural components of the generated images are corrected. Specifically, we see that unnatural depictions of human hands, and incorrect renderings of the text are corrected in CFG++, a long-standing research question in and of its own (Podell et al., 2023; Pelykh et al., 2024; Chen et al., 2023).

In Fig. 8, we visualize multiple images generated by CFG++ as we increase the guidance scale λ , illustrating a smooth transition from unconditional to highly conditional sampling. Specifically, at higher guidance scales, the target concept is more pronounced, with less emphasis on noisy, unrelated elements. This results in images that more closely reflect the specified text conditions. For example, in the second row, the images increasingly resemble a "painting by Van Gogh," demonstrating how the generated visuals align more significantly with the given textual description as the guidance scale increase to 1.

4.2 DIFFUSION IMAGE INVERSION AND EDITING

We further explore the effect of CFG++ on DDIM inversion (Dhariwal & Nichol, 2021), where the source image is reverted to a latent vector that can reproduce the original image through generative

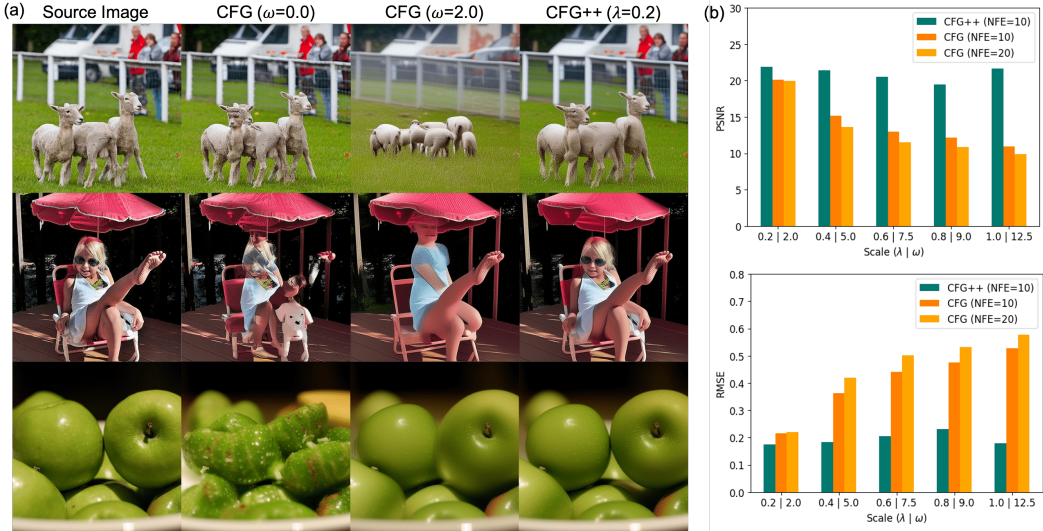


Figure 9: Real image DDIM inversion results by CFG and CFG++ scales using SDv1.5. (a) Reconstructed samples after inversion. (b) Quantitative comparison between CFG and CFG++.

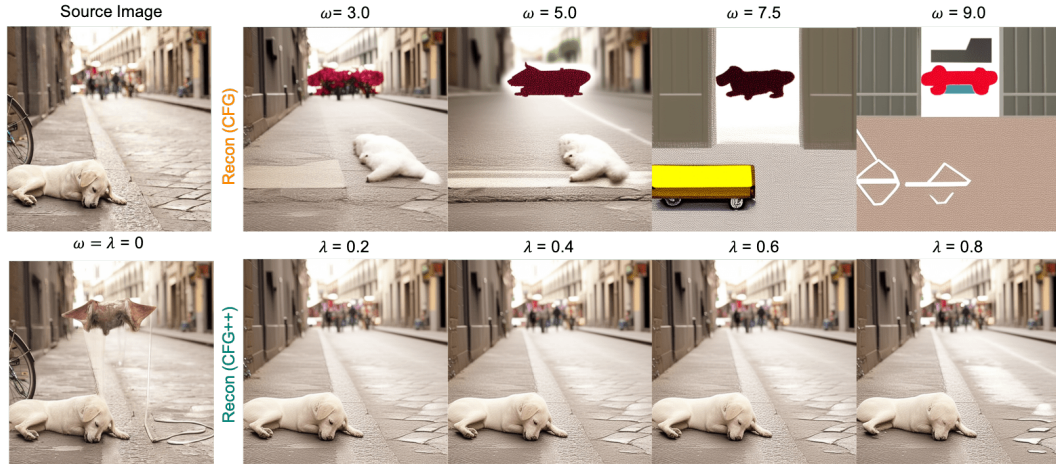


Figure 10: Real image inversion results at various CFG and CFG++ scales using SDv1.5. The image is from COCO dataset. We use the text prompt “a white dog is sleeping on a street and a bicycle” during the inversion.

process. DDIM inversion is well-known to break down in the usual CFG setting as CFG magnifies the accumulated error of each inversion step (Mokady et al., 2023), violating local linearization assumptions (Wallace et al., 2023). Remarkably, CFG++ may mitigate this issue. This improves inversion and enables better image editing compared to inversion with the original CFG. We evaluate our method following the experimental setups in Park et al. (2024) and Kim et al. (2024). More details follow.

Diffusion Image Inversion. Using the matched set of scales for ω and λ , we demonstrate the effect of CFG++ on the diffusion image inversion task. Specifically, we reconstruct the images after inversion and evaluate it through PSNR and RMSE, following the methodology of Wallace et al. (2023). In Fig. 9, we illustrate the reconstructed examples (9a) from a real image from COCO data set and computed metrics (9b) for 5k COCO-2014 (Lin et al., 2014) validation set. Both qualitative and quantitative evaluation demonstrate a consistent improvement on reconstruction performance induced by CFG++. Notably, DDIM inversion with CFG++ leads to consistent reconstruction of the source image across all guidance scales, while DDIM inversion with CFG fails to reconstruct it, as shown in Fig. 10 for another real image.

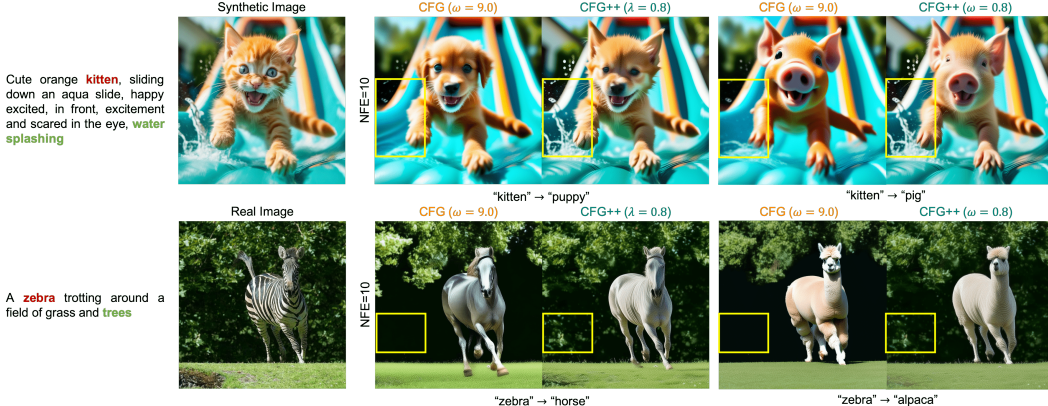


Figure 11: Comparison on image editing via DDIM inversion using SD v1.5: (top) synthetic image editing, (bottom) real image editing.

Image Editing. Fig. 11 compares the image editing result using CFG and CFG++ followed by image inversion. In the image editing stage, a word in the source text on the left side is swapped with the target concept, and this modified text is used as condition for sampling. For both synthetic and real images, CFG++ successfully edits the target concept while preserving other concepts, such as background. In particular, the water splashing or brush in the background, which tend to disappear in the conventional CFG, are maintained through the inversion process by CFG++. This emphasizes CFG++’s superior ability to retain specific scene elements that are frequently lost in the standard CFG approach.

4.3 TEXT-CONDITIONED INVERSE PROBLEMS

Inverse problem involves restoring the original data \mathbf{x} from a noisy measurement $\mathbf{y} = \mathcal{A}(\mathbf{x}) + \mathbf{n}$, where \mathcal{A} represents an imaging operator introduces distortions (e.g, Gaussian blur) and \mathbf{n} denotes the measurement noise. Diffusion inverse solvers (DIS) address this challenge by leveraging pre-trained diffusion models as implicit priors and performing posterior sampling $\mathbf{x} \sim p(\mathbf{x}|\mathbf{y})$. Methods that leverage latent diffusion have gained recent interest (Rout et al., 2024; Song et al., 2024), but leveraging texts for solving these problems remains relatively underexplored (Chung et al., 2023b; Kim et al., 2023). One of the main reasons for this is that naively using CFG on top of latent DIS leads to diverging samples (Chung et al., 2023b). Several heuristic modifications such as null prompt optimization (Kim et al., 2023) with modified sampling schemes were needed to mitigate this drawback. This naturally leads to the question: Is it possible to leverage CFG guidance as a plug-and-play component of existing solvers? Here, we answer this question with a positive by showing that CFG++ enables the incorporation of text prompts into a standard solver. Specifically, we focus on comparing the performance of PSLD (Rout et al., 2024) combined with CFG and CFG++ in solving linear inverse problems. This evaluation utilizes the FFHQ (Karras et al., 2019) 512x512 dataset and the text prompt "a high-quality photo of a face". Further details about the experimental settings can be found in the Appendix A.

As shown in Tab. 2, our method mostly outperforms both the vanilla PSLD and PSLD with CFG. The superiority is also evident from the Fig. 12, where CFG++ consistently delivers high-quality reconstructions across all tasks. PSLD with CFG often suffer from artifacts and blurriness. Conversely, CFG++ achieves better fidelity, clearly distinguishing between faces and faithfully reproducing fine details like eyelids and hair texture. For more results, please refer to the Appendix B.

Method	SR (x8)			Deblur (motion)			Deblur (gauss)			Inpaint		
	FID ↓	LPIPS ↓	PSNR ↑	FID ↓	LPIPS ↓	PSNR ↑	FID ↓	LPIPS ↓	PSNR ↑	FID ↓	LPIPS ↓	PSNR ↑
PSLD	46.24	0.413	24.41	97.51	0.500	21.83	41.65	0.388	26.88	10.27	9.36	30.15
PSLD + CFG	41.24	0.394	24.91	91.90	0.493	22.29	41.52	0.390	26.94	9.36	0.055	30.27
PSLD + CFG++ (ours)	36.58	0.385	24.87	65.67	0.482	21.93	39.85	0.400	26.90	9.78	0.052	30.31

Table 2: Quantitative comparison (FID, LPIPS, PSNR) of PSLD, PSLD with CFG, and PSLD with CFG++ on Latent Diffusion Inverse Solver.

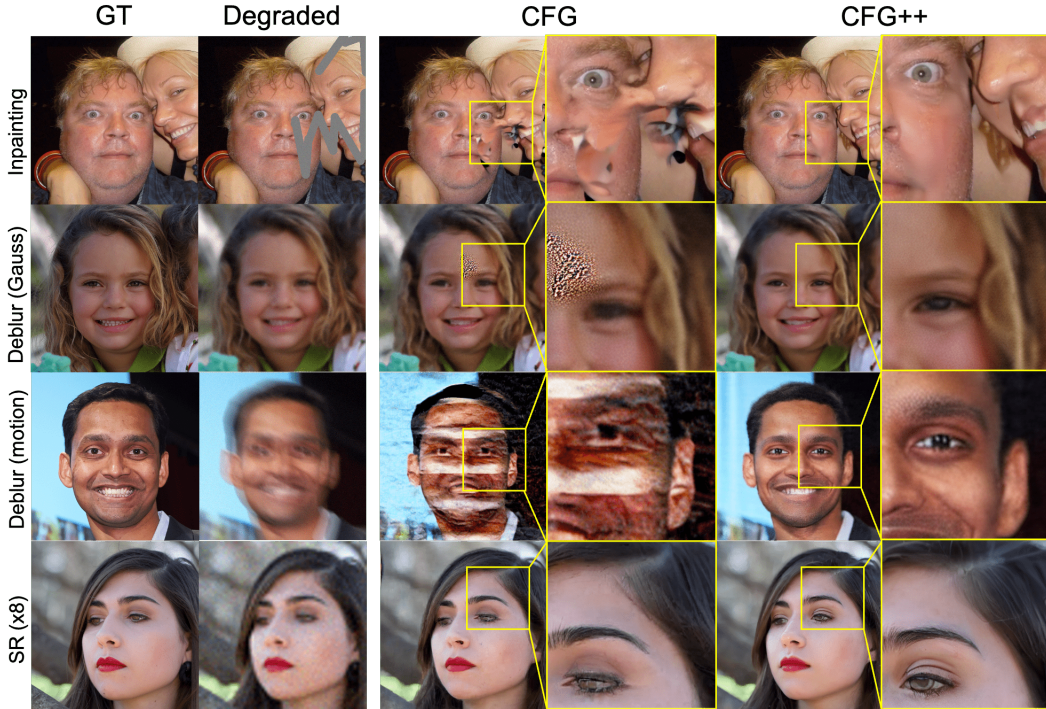


Figure 12: Qualitative comparison on various inverse problems using PSLD (Rout et al., 2024) under CFG and CFG++.

5 RELATED WORKS AND DISCUSSION

Related works. Kynkänniemi et al. (2024) observed that applying CFG guidance at the earlier stages of sampling always led to detrimental effects and drastically reduced the diversity of the samples. The guidance at the later stages of sampling had minimal effects. Drawing upon these observations, it was empirically shown that applying CFG only in the limited time interval near the middle led to the best performance. Similar observations were made in the SD community (Howard & Prashanth, 2022; Birch, 2023) in adjusting the guidance scale across t . These findings are orthogonal to ours in that these methods keep the sampling trajectory the same and try to empirically adjust the strength of the guidance, while we aim to design a different trajectory.

Implications. In several studies, attempts at designing a better trajectory of the generative path were made (Liu et al., 2023a; Lipman et al., 2023). As diffusion models can only estimate the tangent vector of the trajectory at time t , it is now a well regarded consensus that minimizing the curvature of the trajectory leads to faster sampling (Liu et al., 2023a; Lee et al., 2023) and better distillation results (Liu et al., 2023b). In this regard, the excessively high curvature and oscillating behavior of CFG with high guidance scales would hamper the performance of fast sampling and distillation, which was constantly reported in the literature as difficulties in extending distillation methods (Salimans & Ho, 2022; Song et al., 2023b) to the latent space (Meng et al., 2023; Luo et al., 2023; Chen et al., 2024a). Straightening the diffusion path prior to distillation with Reflow (Liu et al., 2023a) exhibited much better results than aiming for direct distillation. In this regard, CFG++ can also be considered a better alternative to CFG for enhanced distillation performance.

6 CONCLUSION

This paper revises the most widespread guidance method, classifier-free guidance (CFG), highlighting that a small and reasonable guidance scale, e.g. $\lambda \in [0.0, 1.0]$, might suffice successful guidance with a proper geometric correction. Observing that the original CFG suffers from off-manifold issues during sampling, we propose a simple but surprisingly effective fix: using $\hat{\epsilon}_\phi(x_t)$ instead of $\hat{\epsilon}_c^\omega(x_t)$ in updating x_{t-1} . This change translates the conditional guidance from extrapolating to interpolating between unconditional and conditional sampling trajectories, leading to more interpretable guidance

in contrast to the conventional CFG which heavily relies on heuristic ω scaling. Given that CFG++ mitigates off-manifold issues, it may be beneficial for other downstream applications requiring accurate latent denoised estimate representations, e.g. DIS, as demonstrated in our experiments.

REFERENCES

- Alex Birch. Turning off classifier-free guidance at low noise levels. <https://twitter.com/Birchlabs/status/1640033271512702977>, 2023. Idea mentioned on Twitter.
- Jingye Chen, Yupan Huang, Tengchao Lv, Lei Cui, Qifeng Chen, and Furu Wei. Textdiffuser: Diffusion models as text painters. In *Thirty-seventh Conference on Neural Information Processing Systems*, 2023. URL <https://openreview.net/forum?id=ke3RgcDmf0>.
- Junsong Chen, Yue Wu, Simian Luo, Enze Xie, Sayak Paul, Ping Luo, Hang Zhao, and Zhenguo Li. Pixart-delta: Fast and controllable image generation with latent consistency models. *arXiv preprint arXiv:2401.05252*, 2024a.
- Junsong Chen, Jincheng YU, Chongjian GE, Lewei Yao, Enze Xie, Zhongdao Wang, James Kwok, Ping Luo, Huchuan Lu, and Zhenguo Li. PixArt-a: Fast training of diffusion transformer for photorealistic text-to-image synthesis. In *The Twelfth International Conference on Learning Representations*, 2024b. URL <https://openreview.net/forum?id=eAKmQPe3m1>.
- Hyungjin Chung, Byeongsu Sim, Dohoon Ryu, and Jong Chul Ye. Improving diffusion models for inverse problems using manifold constraints. In Alice H. Oh, Alekh Agarwal, Danielle Belgrave, and Kyunghyun Cho (eds.), *Advances in Neural Information Processing Systems*, 2022. URL <https://openreview.net/forum?id=nJJjv0JDJju>.
- Hyungjin Chung, Jeongsol Kim, Michael Thompson Mccann, Marc Louis Klasky, and Jong Chul Ye. Diffusion posterior sampling for general noisy inverse problems. In *International Conference on Learning Representations*, 2023a. URL <https://openreview.net/forum?id=OnD9zGAGT0k>.
- Hyungjin Chung, Jong Chul Ye, Peyman Milanfar, and Mauricio Delbracio. Prompt-tuning latent diffusion models for inverse problems. *arXiv preprint arXiv:2310.01110*, 2023b.
- Hyungjin Chung, Suhyeon Lee, and Jong Chul Ye. Decomposed diffusion sampler for accelerating large-scale inverse problems. In *The Twelfth International Conference on Learning Representations*, 2024. URL <https://openreview.net/forum?id=DsEhqQtFAG>.
- Prafulla Dhariwal and Alexander Quinn Nichol. Diffusion models beat GANs on image synthesis. In A. Beygelzimer, Y. Dauphin, P. Liang, and J. Wortman Vaughan (eds.), *Advances in Neural Information Processing Systems*, 2021.
- Yilun Du, Conor Durkan, Robin Strudel, Joshua B Tenenbaum, Sander Dieleman, Rob Fergus, Jascha Sohl-Dickstein, Arnaud Doucet, and Will Sussman Grathwohl. Reduce, reuse, recycle: Compositional generation with energy-based diffusion models and mcmc. In *International Conference on Machine Learning*, pp. 8489–8510. PMLR, 2023.
- Bradley Efron. Tweedie’s formula and selection bias. *Journal of the American Statistical Association*, 106(496):1602–1614, 2011.
- Jonathan Ho and Tim Salimans. Classifier-free diffusion guidance. In *NeurIPS 2021 Workshop on Deep Generative Models and Downstream Applications*, 2021. URL <https://openreview.net/forum?id=qw8AKxfYbI>.
- Jonathan Ho, Ajay Jain, and Pieter Abbeel. Denoising diffusion probabilistic models. *Advances in Neural Information Processing Systems*, 33:6840–6851, 2020.
- Jeremy Howard and Rekil Prashanth. Adjusting guidance weight as a function of time. <https://twitter.com/jeremyphoward/status/1584771100378288129>, 2022. Idea mentioned on Twitter.
- Aapo Hyvärinen and Peter Dayan. Estimation of non-normalized statistical models by score matching. *Journal of Machine Learning Research*, 6(4), 2005.

- Zahra Kadkhodaie and Eero P Simoncelli. Stochastic solutions for linear inverse problems using the prior implicit in a denoiser. In A. Beygelzimer, Y. Dauphin, P. Liang, and J. Wortman Vaughan (eds.), *Advances in Neural Information Processing Systems*, 2021. URL <https://openreview.net/forum?id=x5hh6N9bUUb>.
- Tero Karras, Samuli Laine, and Timo Aila. A style-based generator architecture for generative adversarial networks. In *Proceedings of the IEEE/CVF Conference on Computer Vision and Pattern Recognition*, pp. 4401–4410, 2019.
- Tero Karras, Miika Aittala, Timo Aila, and Samuli Laine. Elucidating the design space of diffusion-based generative models. In *Proc. NeurIPS*, 2022.
- Jeongsol Kim, Geon Yeong Park, Hyungjin Chung, and Jong Chul Ye. Regularization by texts for latent diffusion inverse solvers. *arXiv preprint arXiv:2311.15658*, 2023.
- Jeongsol Kim, Geon Yeong Park, and Jong Chul Ye. Dreamsampler: Unifying diffusion sampling and score distillation for image manipulation. *arXiv preprint arXiv:2403.11415*, 2024.
- Tuomas Kynkänniemi, Miika Aittala, Tero Karras, Samuli Laine, Timo Aila, and Jaakko Lehtinen. Applying guidance in a limited interval improves sample and distribution quality in diffusion models. *arXiv preprint arXiv:2404.07724*, 2024.
- Sangyun Lee, Beomsu Kim, and Jong Chul Ye. Minimizing trajectory curvature of ode-based generative models. In *International Conference on Machine Learning*, pp. 18957–18973. PMLR, 2023.
- Yixun Liang, Xin Yang, Jiantao Lin, Haodong Li, Xiaogang Xu, and Yingcong Chen. Lucid-dreamer: Towards high-fidelity text-to-3d generation via interval score matching. *arXiv preprint arXiv:2311.11284*, 2023.
- Tsung-Yi Lin, Michael Maire, Serge Belongie, James Hays, Pietro Perona, Deva Ramanan, Piotr Dollár, and C Lawrence Zitnick. Microsoft coco: Common objects in context. In *Computer Vision-ECCV 2014: 13th European Conference, Zurich, Switzerland, September 6-12, 2014, Proceedings, Part V 13*, pp. 740–755. Springer, 2014.
- Yaron Lipman, Ricky T. Q. Chen, Heli Ben-Hamu, Maximilian Nickel, and Matthew Le. Flow matching for generative modeling. In *The Eleventh International Conference on Learning Representations*, 2023. URL <https://openreview.net/forum?id=PqvMRDCJT9t>.
- Xingchao Liu, Chengyue Gong, and qiang liu. Flow straight and fast: Learning to generate and transfer data with rectified flow. In *The Eleventh International Conference on Learning Representations*, 2023a. URL <https://openreview.net/forum?id=XVjTT1nw5z>.
- Xingchao Liu, Xiwen Zhang, Jianzhu Ma, Jian Peng, et al. Instaflow: One step is enough for high-quality diffusion-based text-to-image generation. In *The Twelfth International Conference on Learning Representations*, 2023b.
- Simian Luo, Yiqin Tan, Longbo Huang, Jian Li, and Hang Zhao. Latent consistency models: Synthesizing high-resolution images with few-step inference. *arXiv preprint arXiv:2310.04378*, 2023.
- Chenlin Meng, Robin Rombach, Ruiqi Gao, Diederik Kingma, Stefano Ermon, Jonathan Ho, and Tim Salimans. On distillation of guided diffusion models. In *Proceedings of the IEEE/CVF Conference on Computer Vision and Pattern Recognition*, pp. 14297–14306, 2023.
- Ron Mokady, Amir Hertz, Kfir Aberman, Yael Pritch, and Daniel Cohen-Or. Null-text inversion for editing real images using guided diffusion models. In *Proceedings of the IEEE/CVF Conference on Computer Vision and Pattern Recognition*, pp. 6038–6047, 2023.
- Geon Yeong Park, Jeongsol Kim, Beomsu Kim, Sang Wan Lee, and Jong Chul Ye. Energy-based cross attention for bayesian context update in text-to-image diffusion models. *Advances in Neural Information Processing Systems*, 36, 2024.

- Suraj Patil, Pedro Cuenca, Nathan Lambert, and Patrick von Platen. Stable diffusion with diffusers. *Hugging Face Blog*, 2022. https://huggingface.co/blog/stable_diffusion.
- Anton Pelykh, Ozge Mercanoglu Sincan, and Richard Bowden. Giving a hand to diffusion models: a two-stage approach to improving conditional human image generation. *arXiv preprint arXiv:2403.10731*, 2024.
- Dustin Podell, Zion English, Kyle Lacey, Andreas Blattmann, Tim Dockhorn, Jonas Müller, Joe Penna, and Robin Rombach. Sdxl: Improving latent diffusion models for high-resolution image synthesis. *arXiv preprint arXiv:2307.01952*, 2023.
- Ben Poole, Ajay Jain, Jonathan T. Barron, and Ben Mildenhall. Dreamfusion: Text-to-3d using 2d diffusion. *arXiv*, 2022.
- Robin Rombach, Andreas Blattmann, Dominik Lorenz, Patrick Esser, and Björn Ommer. High-resolution image synthesis with latent diffusion models. In *Proceedings of the IEEE/CVF Conference on Computer Vision and Pattern Recognition*, pp. 10684–10695, 2022.
- Litu Rout, Negin Raoof, Giannis Daras, Constantine Caramanis, Alex Dimakis, and Sanjay Shakkottai. Solving linear inverse problems provably via posterior sampling with latent diffusion models. *Advances in Neural Information Processing Systems*, 36, 2024.
- Chitwan Saharia, William Chan, Huiwen Chang, Chris Lee, Jonathan Ho, Tim Salimans, David Fleet, and Mohammad Norouzi. Palette: Image-to-image diffusion models. In *ACM SIGGRAPH 2022 conference proceedings*, pp. 1–10, 2022.
- Tim Salimans and Jonathan Ho. Progressive distillation for fast sampling of diffusion models. In *International Conference on Learning Representations*, 2022. URL <https://openreview.net/forum?id=TIdIXIpzhoI>.
- Christoph Schuhmann, Romain Beaumont, Richard Vencu, Cade Gordon, Ross Wightman, Mehdi Cherti, Theo Coombes, Aarush Katta, Clayton Mullis, Mitchell Wortsman, et al. Laion-5b: An open large-scale dataset for training next generation image-text models. *Advances in Neural Information Processing Systems*, 35:25278–25294, 2022.
- Bowen Song, Soo Min Kwon, Zecheng Zhang, Xinyu Hu, Qing Qu, and Liyue Shen. Solving inverse problems with latent diffusion models via hard data consistency. In *The Twelfth International Conference on Learning Representations*, 2024. URL <https://openreview.net/forum?id=j8hdRq0UhN>.
- Jiaming Song, Chenlin Meng, and Stefano Ermon. Denoising diffusion implicit models. In *9th International Conference on Learning Representations, ICLR*, 2021a.
- Jiaming Song, Arash Vahdat, Morteza Mardani, and Jan Kautz. Pseudoinverse-guided diffusion models for inverse problems. In *International Conference on Learning Representations*, 2023a. URL https://openreview.net/forum?id=9_gsMA8MRKQ.
- Yang Song, Jascha Sohl-Dickstein, Diederik P. Kingma, Abhishek Kumar, Stefano Ermon, and Ben Poole. Score-based generative modeling through stochastic differential equations. In *9th International Conference on Learning Representations, ICLR*, 2021b.
- Yang Song, Prafulla Dhariwal, Mark Chen, and Ilya Sutskever. Consistency models. *arXiv preprint arXiv:2303.01469*, 2023b.
- Bram Wallace, Akash Gokul, and Nikhil Naik. EDICT: Exact diffusion inversion via coupled transformations. In *Proceedings of the IEEE/CVF Conference on Computer Vision and Pattern Recognition*, pp. 22532–22541, 2023.
- Zhengyi Wang, Cheng Lu, Yikai Wang, Fan Bao, Chongxuan Li, Hang Su, and Jun Zhu. Proflifdreamer: High-fidelity and diverse text-to-3d generation with variational score distillation. *Advances in Neural Information Processing Systems*, 36, 2024.
- Junzhe Zhu, Peiye Zhuang, and Sanmi Koyejo. Hifa: High-fidelity text-to-3d generation with advanced diffusion guidance. In *The Twelfth International Conference on Learning Representations*, 2023.

A EXPERIMENTAL DETAILS

A.1 TEXT-CONDITIONED INVERSE PROBLEMS

Problem settings. We evaluate our approach across following degradation types: 1) Super-resolution with a scale factor of x8, 2) Motion deblurring from an image convolved with a 61 x 61 motion kernel, randomly sampled with an intensity value 0.3², 3) Gaussian deblurring from an image convolved with a 61 x 61 kernel with an intensity value 0.5, and 4) Inpainting from 10-20% free-form masking, as implemented in (Saharia et al., 2022). In inpainting evaluations, regions outside the mask are overlaid with the ground truth image.

Datasets, Models. For evaluation, we use the FFHQ (Karras et al., 2019) 512x512 dataset and follow (Chung et al., 2023a) by selecting the first 1,000 images for testing. For the pre-trained latent diffusion model including baseline methods, we choose SD v1.5 trained on the LAION dataset. As a baseline for latent DIS, we consider PSLD (Rout et al., 2024). It enforces fidelity by projecting onto the subspace of \mathcal{A} during the intermediate step between decoding and encoding, in conjunction with the DPS (Chung et al., 2023a) loss term. For gradient updates in both vanilla PSLD and PSLD with CFG, we use static step sizes of $\eta = 1.0$ and $\gamma = 0.1$ as recommended in (Rout et al., 2024). For CFG scale ω , we applied the corresponding scales that we found to be corresponded for CFG++ scale λ . Please refer to the Tab. 3 for the hyperparameters used for PSLD with CFG++.

	SR(x8)	Deblur(motion)	Deblur(gauss)	Inpaint
η	1.3	0.4	1.0	1.0
γ	0.1	0.025	0.12	0.1
λ	0.1	0.2	0.2	0.6
ω	1.5	2.0	2.0	7.5

Table 3: Hyperparameters for PSLD (Rout et al., 2024) with CFG++ and corresponding CFG scale ω .

B FURTHER EXPERIMENTAL RESULTS

B.1 T2I

Since the range of guidance scales for CFG and CFG++ is different, we matched the guidance values of ω and λ for comparison by computing the LPIPS distance using the same seed. Fig. 17 displays an example of generated images given the same text prompt and seed, while varying the guidance scale.

Fig. 13 shows the clean estimates at each diffusion sampling time t , computed using Tweedie’s formula, both with and without CFG. It is evident that the original CFG induces significant error, particularly at earlier times, leading to off-manifold samples. However, the revised CFG addresses this issue by adjusting the DDIM re-noising step and the guidance scale.

B.2 REAL IMAGE EDITING

In Fig. 14-16, we provide qualitative comparison on real image editing via DDIM inversion with CFG and CFG++. For the DDIM inversion stage, we use "a photography of [source concept]" as conditioning prompt. For the sampling stage, we swap [source concept] to [target concept] and use it as conditioning prompt for generation. For example, in Fig. 14, we set [source concept] to "dog" and [target concept] to "cat". For all experiments, we set the guidance scale as $\omega = 9.0$ and $\lambda = 0.8$ as described in the main paper. The comparison demonstrates that CFG++ successfully edits the given image which was not enabled for CFG. This results also support our claim on reduced error during DDIM inversion by CFG++.

B.3 TEXT-CONDITIONED INVERSE PROBLEMS

In Fig. 18-21, we display additional qualitative comparison for text-conditioned inverse problem solver with CFG and CFG++. Experiments are conducted with FFHQ (512x512) validation set and CFG++ consistently leads to better reconstruction of true solution for various tasks.

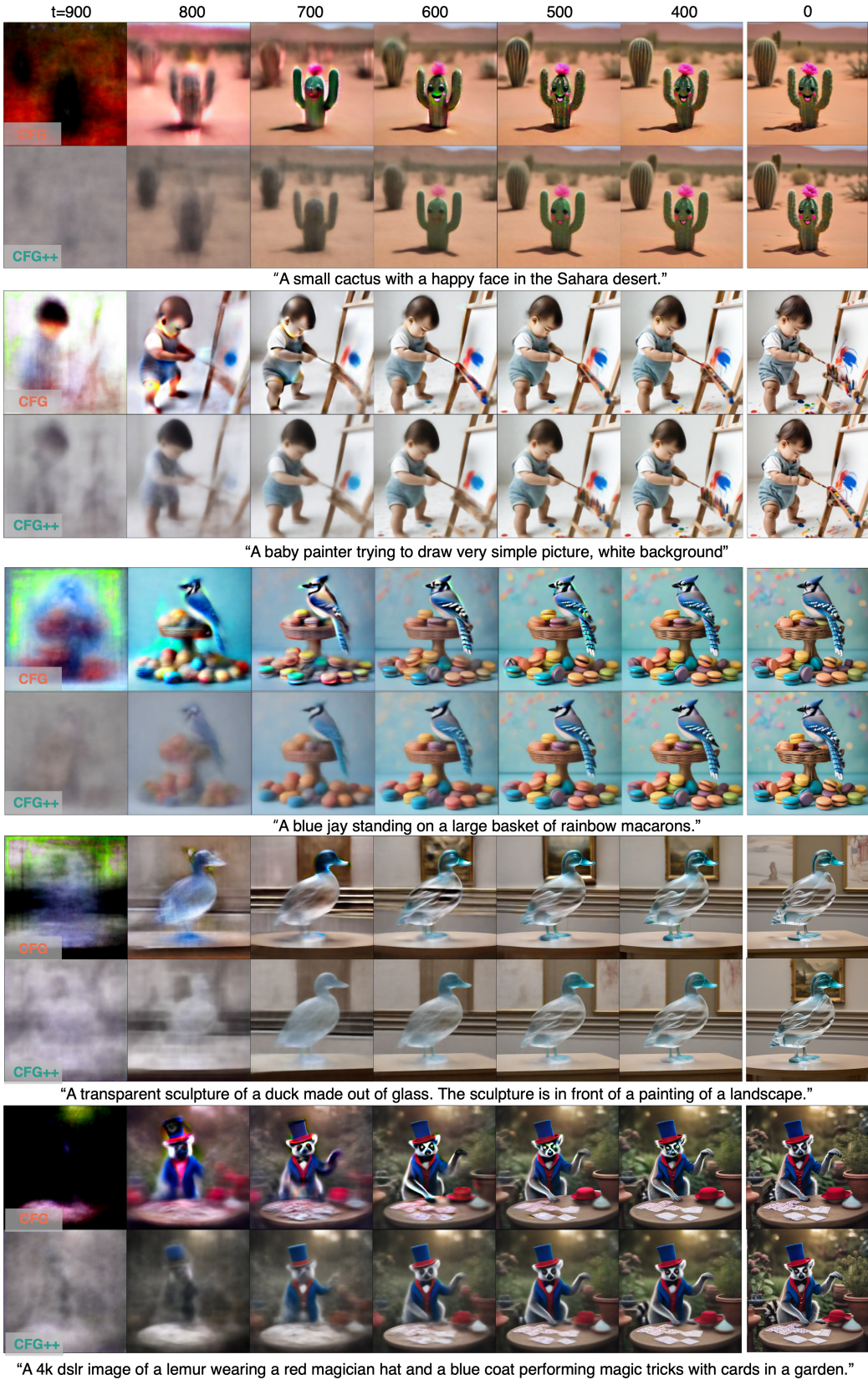


Figure 13: The discrete evolution of the posterior mean in CFG and CFG++. Denoised estimates in latent space are decoded into pixel space at each timestep using SDXL.



Figure 14: Comparison on real image editing via DDIM inversion and SDXL. Cat → Dog.

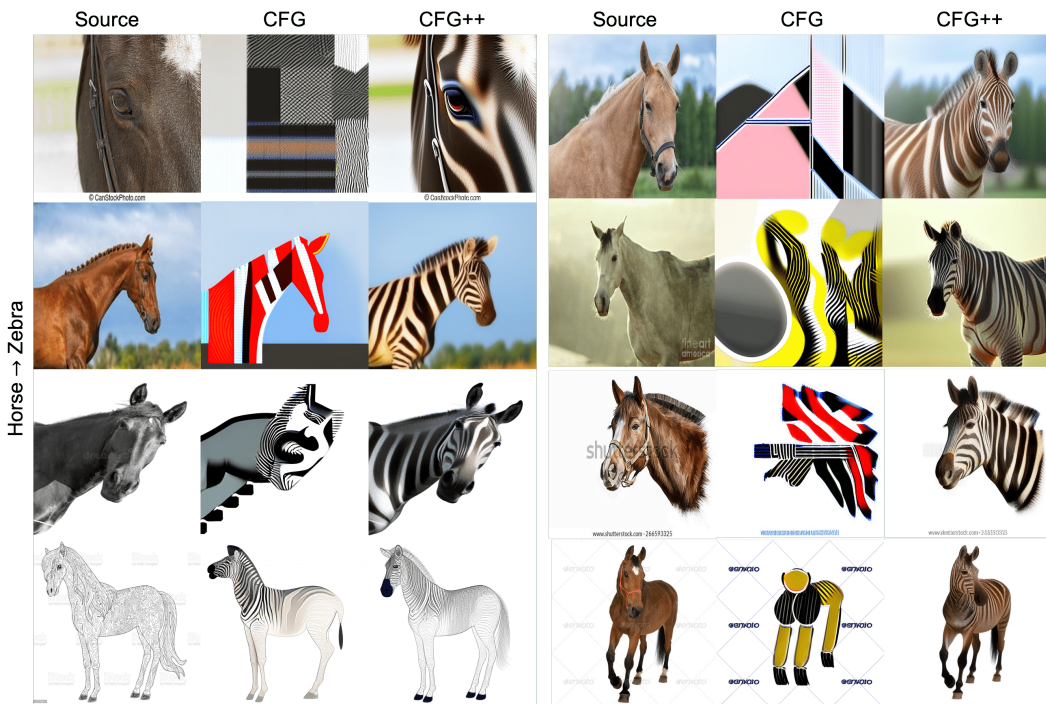


Figure 15: Comparison on real image editing via DDIM inversion and SDXL. Horse → Zebra.



Figure 16: Comparison on real image editing via DDIM inversion and SDXL. Cat → Cat with glasses.

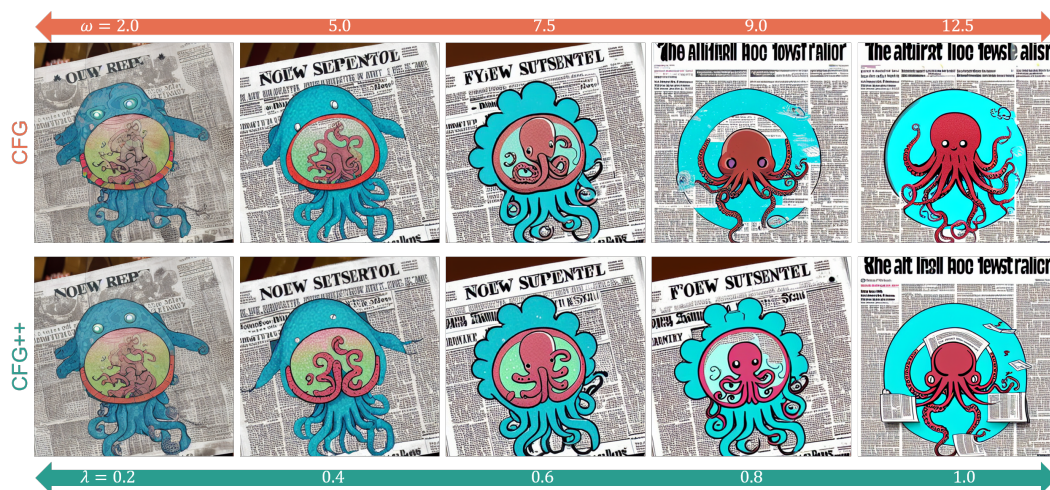


Figure 17: Example of generated images with various guidance scales.



Figure 18: Results of PSLD using CFG and CFG++ on the FFHQ dataset at Super-Resolution (x8).

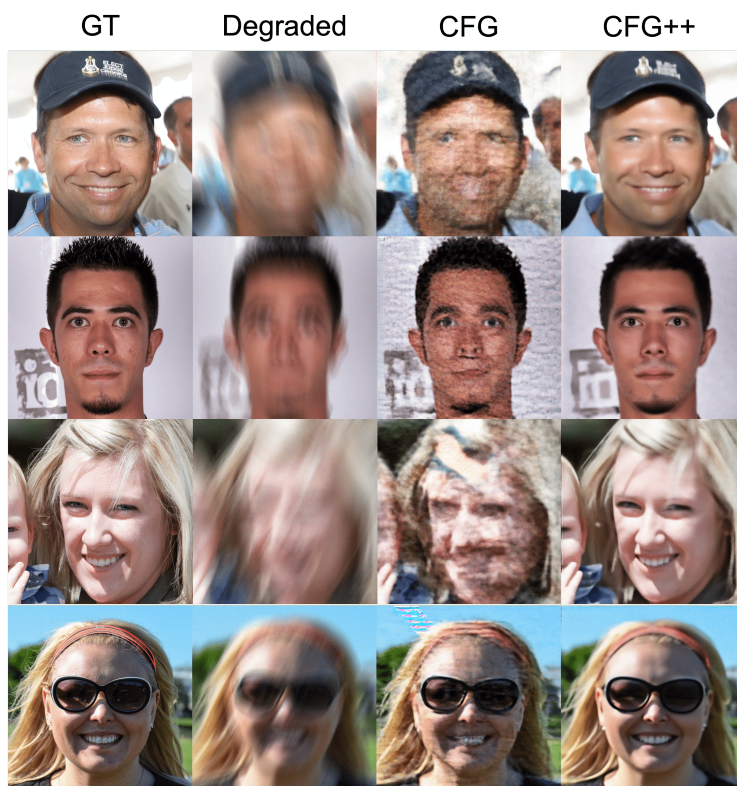


Figure 19: Results of PSLD using CFG and CFG++ on the FFHQ dataset at Motion Deblurring.

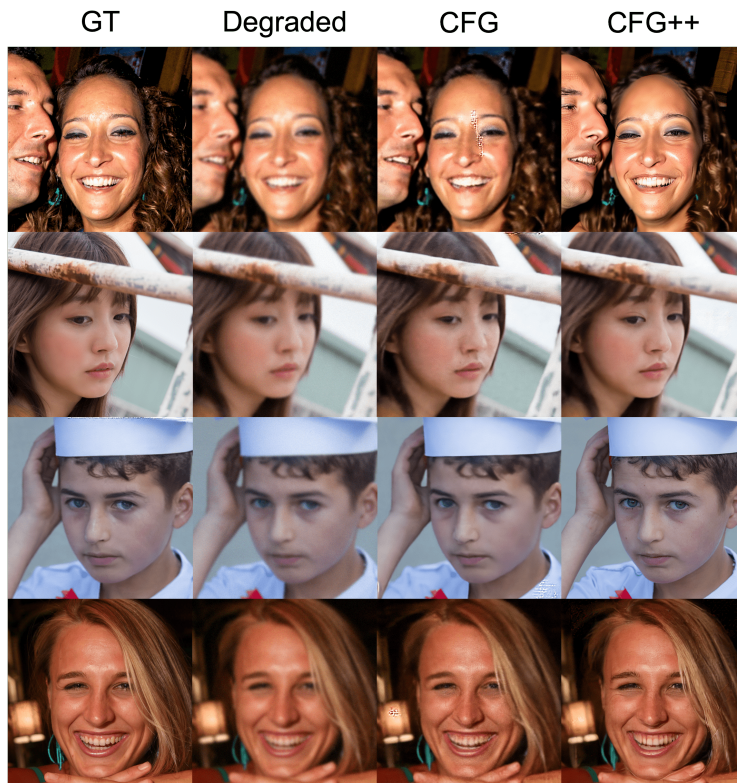


Figure 20: Results of PSLD using CFG and CFG++ on the FFHQ dataset at Gaussian Deblurring.

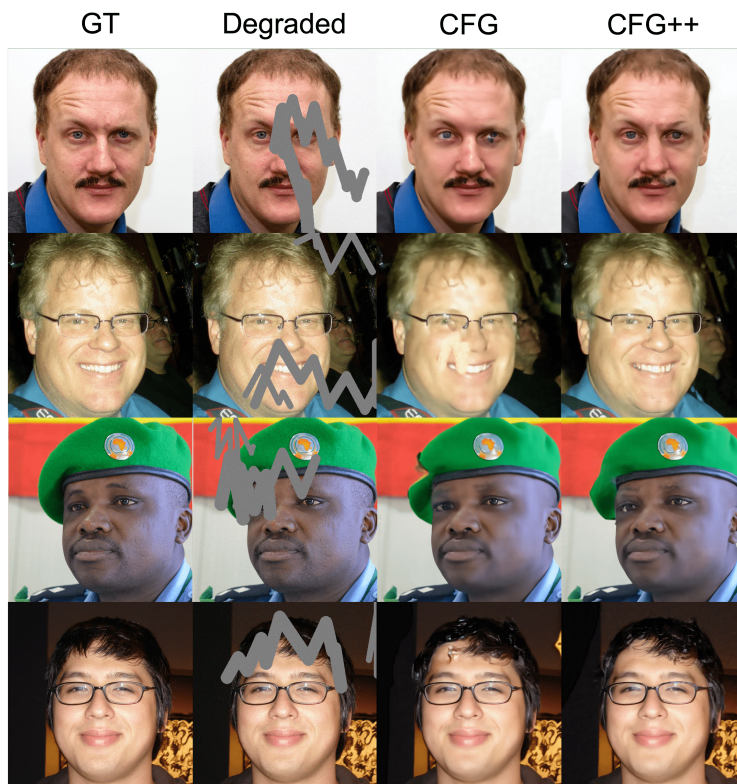


Figure 21: Results of PSLD using CFG and CFG++ on the FFHQ dataset at Inpainting.